Proceedings of the 9th International Conference on Fluid Flow, Heat and Mass Transfer (FFHMT'22)
Niagara Falls, Canada – June 08-10, 2022
Paper No. 198
DOI: 10.11159/ffhmt22.198

Numerical Approach in Determination of Thermophysical Material Properties in Decomposition of Lumpy Dolomite Particles

Waliyu Abdulkadir Aliyu[1], Md. Ishtiaque Hossain[1], Eckehard Specht[1]
[1]Institute of Fluid Dynamics and Thermodynamics, University of Magdeburg
Universitaetsplatz 2, 39106 Magdeburg, Germany
waliyu.aliyu@ovgu.de; md2.hossain@st.ovgu.de; eckehard.specht@ovgu.de

Abstract **-** We report on the decomposition of cylindrical dolomite ($CaMg(CO_3)_2$) particles through the two steps decomposition scheme with the objective of determining the thermophysical properties of the decomposition product in each step. Samples of size 24 and 32 mm were decomposed in a tube furnace at constant ambient temperature and at atmospheric pressure. By means of weighing and simultaneous temperature measurement, the decomposition behaviour is studied. Obtained decomposition behaviour are remarkably similar to that reported for pure magnesite in step 1 and pure limestone in step 2. Thermophysical properties of $MgO{\cdot}CaCO_3$ and MgO·CaO at different temperatures were estimated by numerically solving the heat and mass transfer equations describing the process, based on the shrinking core model, using the finite difference approach. The reaction coefficient and thermal conductivity of $MgO{\cdot}CaCO_3$ vary from 0.0040 to 0.0085 m/s and 0.79 to 0.92 W/m.K respectively and the permeability is approximately 1×10^{-12} m^2. The reaction coefficient and pore diffusivity of MgO·CaO are in the range of 0.013 - 0.014 m/s and 1.7×10^{-5} – 3.0×10^{-5} m^2/s and the thermal conductivity is approximately 0.8 W/m.K.

Keywords**:** Dolomite decomposition; Thermal conductivity; Reaction coefficient; Pore diffusivity; Permeability; Finite difference method.

1. Introduction

Dolomitic lime is a significant raw material for several industrial and chemical processes. The usage of dolomitic lime (MgO·CaO) has been traced as far back to ancient masonry where it was applied as a binder for mortars [1]. Dolomitic lime has found application in processes for example as a precipitant in the manufacture of magnesia, as a component in the production of calcium magnesium acetate (CMA), in the fabrication of high purity refractory products, as a component in the industrial production of Portland cement [2]. Refs. [1], [3], [4] have shown that the use MgO·CaO reduces drastically the carbonation reactivity decline with increasing number of calcination/carbonation cycles in calcium looping system. Dolomitic lime is generally produced from the calcination of dolomite ($Mg{\cdot}Ca(CO_3)_2$) in a variety of reactors e.g. shaft or rotary kilns, with the release of CO_2.

The decomposition of Dolomite has been extensively studied [5] – [8]. Two pathways to the formation of MgO·CaO have been proposed. The first involves the formation of MgO·CaO in a single stage in the presence of less than 10% CO_2 concentration. Above this concentration, the decomposition of dolomite takes place in two stages. Step 1 represents dolomite decomposition with the release of CO_2 from the carbonate ions linked with magnesium part of the dolomitic structure leading to the formation of magnesium oxide (MgO) and calcium carbonate ($CaCO_3$) and step 2 represents the subsequent decomposition of $CaCO_3$ releasing CO_2. The decomposition of dolomite just like magnesite and calcite involves five processes; heat transfer to the surface of the solid sample, heat conduction from the surface of the sample to the reaction layer, chemical reaction leading to the evolution of CO_2, mass diffusion of released CO_2 through the oxide pores to the solid surface and finally mass transfer to the ambient. To understand the decomposition process it is imperative to know what the transport parameters (mass and heat transfer coefficient) and thermophysical material properties of lime (thermal conductivity, reaction coefficient and pore diffusivity). The former can be obtained from the numerous study that has been done for flows around solid bodies. The latter on the other hand is difficult to measure in the lime layer during calcination.

The decomposition studies carried out by other authors has been on dolomite particles in millimetre or micrometre ranges. These sizes however are firstly, not applicable in industrial kilns and secondly ignore the influence of pore diffusivity, thermal conduction and heat as well as mass transfer coefficient.

The focus of this work is to determine the thermal conductivity, pore diffusivity and reaction coefficient and their temperature dependence for centimetre sized cylindrical dolomite samples following the two steps decomposition scheme. Ref. [9] proposed a simplified analytical method for estimating these material properties which takes account all the aforementioned five processes but strongly depends on the reaction front temperature being constant during the decomposition reaction, which as will be shown varies by about 15°C and thus the method is somewhat inaccurate. The approach of this study is to numerically solve the heat and mass balance equations involved using finite difference approach.

2. Decomposition Model Description

The decomposition process of dolomite is an endothermic topochemical reaction which at high CO_2 partial pressure takes place in two stages [10] – [11], represented by the equations:

Stage 1:

$$CaMg(CO_3)_2\ (s) + \Delta H_R \rightarrow MgO \cdot CaCO_3\ (s) + CO_2(g) \uparrow \quad \Delta\widetilde{H}_R = 117\ kJ/mol \tag{1}$$

Stage 2:

$$MgO \cdot CaCO_3\ (s) + \Delta H_R \rightarrow MgO \cdot CaO(s) + CO_2(g) \uparrow \qquad \Delta\widetilde{H}_R = 164\ kJ/mol \tag{2}$$

In the reactions above, $\Delta\widetilde{H}_R$ represents the endothermic heat of reaction. The two stages of dolomite decomposition can be described using a partially decomposed spherical carbonate piece, schematically shown in Fig. 1a along with temperature and CO_2 partial pressure profiles. The sample is comprised of an unreacted dense core of carbonate enclosed by a porous oxide layer as conversion of material takes place as a phase layer beginning from the surface moving into the sample to the core. In the calcination reactor with a surrounding temperature T_{amb}, there is a combined radiation and convection heat transfer (α) to the sample surface with a temperature T_s. Heat traverses the oxide layer through conduction (λ_{ox}) to the reaction front, where the temperature is T_f. In the course of the decomposition process, heat flow to the unreacted core is slight as the enthalpy is much higher than the internal energy, hence the core temperature is approximately equal to the temperature at the reaction front. With the supply of heat, chemical reaction (k) ensues, driving force of which is the deviation of CO_2 partial pressure from equilibrium ($p_{eq} - p_f$). The CO_2 released diffuses (D_p) through the pores of the oxide layer to the surface and via convection (β) enters the sample surrounding where the CO_2 partial pressure p_{amb} exists. There is thus an interconnection amongst all four physical transport processes and the chemical kinetics at the reaction front.

Ref. [9] developed 1-D shrinking core model to determine the decomposition behaviour of limestone and magnesium carbonate particles, assuming an ideal sample geometry (spheres, cylinder or plate), a sample with a homogeneous chemical and structural composition and a heat supply that is symmetrical. Also assumed is that a smooth reaction front is formed as the reaction starts from the solid surface and proceeds continuously into the interior. This assumption is true macroscopically, however scanning electron microscopy (SEM) [12] show that the edges of the individual crystals are the favoured locations where the reaction starts, and as such the actual reaction layer is a bit larger than the assumed smooth surface (this variation is accounted for in the reaction coefficient (k)).

The coupled 1-D heat equation [13] describing the decomposition process written in cylindrical coordinates is:

$$\rho \cdot c_p \cdot \frac{\partial T}{\partial t} = \lambda \cdot \left(\frac{1}{r} \cdot \frac{\partial T}{\partial r} + \frac{\partial^2 T}{\partial r^2}\right) - \Delta H_R \cdot \dot{M}_{v,CO_2} \tag{3a}$$

where ρ is the sample density (kg/m^3), c_p is specific heat capacity (J/kg·K), λ is thermal conductivity (W/m·K), ΔH_R is reaction enthalpy (J/kg) and $\dot{M}_{v,CO_2}$ is CO_2 mass rate per unit volume (kg/s·m^3).

The relation between equilibrium pressure (p_{eq}) and temperature is given by the thermodynamic relation below;

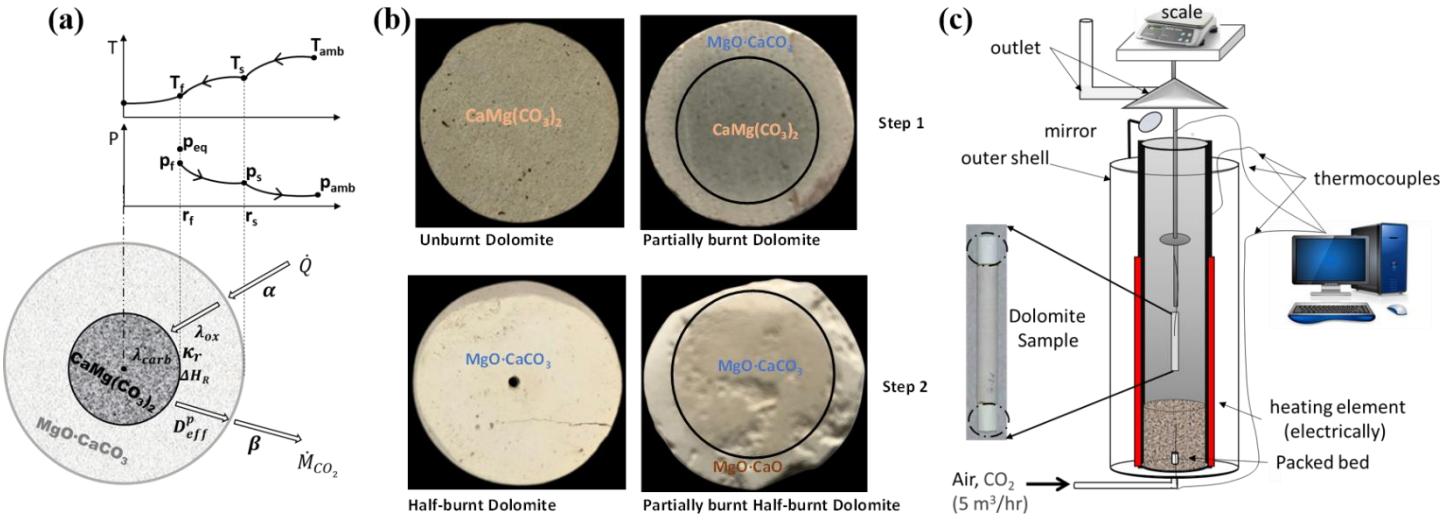

Fig. 1: (a) Schematic of partially decomposed dolomite sample showing an unreacted dense core enclosed by a porous oxide layer describing the decomposition mechanism along with temperature and CO_2 partial pressure. (b) Photos of samples taken for steps 1 and 2 to show the reaction layer moves from the surface to the core. (c) Schematic of the experimental set-up for thermogravimetric experiment.

$$p_{eq} = p_{eq_0} \cdot exp\left(\frac{-\Delta\tilde{H}_R}{\tilde{R} \cdot T}\right) \tag{5}$$

where $\Delta\tilde{H}_R$ and p_{eq_0} are respectively the molar reaction enthalpy (J/mol) and pre-exponential coefficient (N/m^2).

At the reaction front, CO_2 is released with the driving force for the reaction being the deviation of the front pressure from equilibrium and the mass rate is written as:

$$\dot{M}_{CO_2} = \frac{k_r}{R_{CO_2} \cdot T_f} \cdot 2\pi r_f L \cdot (p_{eq} - p_f) \tag{6}$$

where k_r is the reaction rate coefficient (m/s), r_f is the radius of the reaction front layer (m), T_f is the temperature at the reaction front layer (K), L is the sample length (m), R_{CO_2} is CO_2 individual gas constant (J/kg·mole) and p_f is CO_2 partial pressure at the reaction front (bar).

The mass rate of flow of CO_2 through the pores of the oxide layer is given in step 1 by Eq. (7) which accounts for bulk flow of CO_2 through the pores of the oxide layer caused by high pressure gradient between the reaction front and the sample surface (Darcy flow) and in step 2 by Eq. (8) which accounts for both mass diffusion of CO_2 and the additional flow of CO_2 as a result of continuous evolvement at the reaction interface due to chemical reaction (Stefan flow) [13].

$$\dot{M}_{CO_2} = \frac{k \cdot \rho}{\mu} \cdot \frac{2\pi L}{\ln\left(\frac{r_s}{r_f}\right)} \cdot (p_f - p_s) \tag{7}$$

$$\dot{M}_{CO_2} = \frac{P \cdot D_p}{R_{CO_2}.T_f} \cdot \frac{2\pi L}{\ln\left(\frac{r_s}{r_f}\right)} \cdot \ln\left(\frac{P - p_s}{P - p_f}\right) \tag{8}$$

where k is the permeability of the oxide layer (m^2), μ is the dynamic viscosity of CO_2 ($N.s/m^2$), P is the total pressure (N/m^2), D_p is the pore diffusion coefficient (m^2/s), p_s is CO_2 partial pressure at the sample surface and r_s is the sample radius (m).

The mass transfer rate of CO_2 from the surface of the solid to the ambient is:

$$\dot{M}_{CO_2} = \frac{\beta}{R_{CO_2} \cdot T_f} \cdot 2\pi r_s L \cdot (p_s - p_{amb}) \tag{9}$$

where β is the mass transfer coefficient (m/s) and p_{amb} is CO_2 partial pressure in the surrounding (N/m^2).

The reaction front is tracked from mass balance and the mass flux is set by the expression:

$$\dot{M}_{CO_2} = -K_{CO_2} \cdot \frac{dr_f}{dt} \cdot 2\pi r_f L \tag{10}$$

where K_{CO_2} is the concentration of CO_2 in either components of dolomite.

The conversion degree X is given by:

$$X = \frac{M_{CO_2}(t)}{M_{CO_2}(t=0)} = 1 - \left(\frac{r_f}{r_s}\right)^2 \tag{11}$$

The numerical solution of the partial differential Eq. (6) together with the algebraic solution of Eqs. (5) – (11), the core temperature and conversion profiles can be simulated and with comparison with experimentally measured profiles, the thermo physical material properties determined.

3. Experimental Method

Fig. 1c is the schematic of the experimental set up for the thermographimetric study of dolomite decomposition. Cylindrical dolomite samples (38% $MgCO_3$, 56% $CaCO_3$; 2370 kg/m^3) were decomposed at different conditions in an electrically heated furnace, operated at constant temperature. K-type (NiCr-NiAl) thermocouples were fixed different positions on the furnace wall to measure the temperature. The sample was decomposed in pure CO_2 for step 1 following Eq. (1), the product was then removed from the furnace and allowed to cool naturally to room temperature. The cool product was then put back into the furnace and decomposed in air for step 2 according to Eq. (2). To measure the weight loss and hence the conversion degree, the sample was hung on a weighing balance. A hole, 1mm in diameter and 3mm in length, was drilled in the centre of the sample where a K-type (NiCr-Ni) thermocouple is inserted to measure the core temperature. For the transport process to be treated as 1-D in radial direction, it was ensured that the length of the sample was more than 5 times its diameter and both ends of the sample were insulated. Gas (CO_2/air) with a flow rate of 5 m^3/hr was introduced into the furnace through a bed of solid particles (3mm inert alumina balls) from the bottom to allow for proper distribution of gas around the sample. Hot gas is then sucked off from the top of the furnace to prevent accumulation of CO_2 hence keeping the partial pressure of CO_2 in the ambient constant.

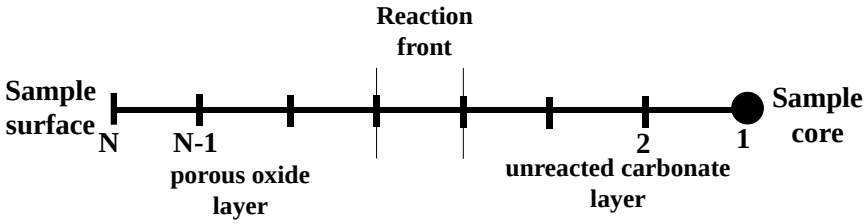

Fig. 2: 1-D discretization of the spatial domain

4. Solution Methodology

The Finite Difference Method (FDM) is used to numerically solve the 1-D partial differential equation (Eq. (3)) which describes the decomposition process. Fig. 2 is the 1-D discretization of the spatial domain with N number of elements. Eq. (3) is subject to the following boundary conditions:

At the solid surface, $r = r_s$ (node N in Fig. 2), combined radiation and convective heat transferred is equal to the heat conducted into the solid:

$$\dot{q} = \left(\sigma \cdot \varepsilon \cdot (T_F^4 - T_s^4) - \alpha_{conv} \cdot (T_s - T_g)\right) = -\lambda \cdot \frac{\partial T}{\partial r} \tag{12}$$

where σ is the Stefan-Boltzmann constant (W/m^2·K^4), ε the emissivity and α_{conv} the heat transfer coefficient (W/m^2·K)

At the core of the sample, $r = 0$ (node 1), axisymmetric condition holds (node 1 in Fig. 2);

$$\dot{q} = -\lambda \cdot \frac{\partial T}{\partial r} = 0 \tag{13}$$

At the start of the decomposition process, $t = 0$, the sample temperature is given as room temperature;

$$T(t = 0) = 293\ K \tag{14}$$

The finite difference form of Eq. (3) and Eqs. (12) – (13) are computed as follows:

The time derivative is approximated using the forward difference approach at $r = r_i$;

$$\frac{\partial T}{\partial t} = \frac{T_i^{n+1} - T_i^n}{\Delta t} \tag{15}$$

The central difference approximation is used to evaluate the first and second order spatial terms at $t = n$;

$$\frac{\partial T}{\partial r} = \frac{T_{i+1}^n - T_{i-1}^n}{2\Delta r} \tag{16a}$$

$$\frac{\partial^2 T}{\partial r^2} = \frac{T_{i+1}^n - 2T_i^n + T_{i-1}^n}{\Delta r^2} \tag{16b}$$

Eqs. (15) – (16) are combined to obtain the discretized form of Eq. (6);

$$\frac{T_i^{n+1} - T_i^n}{\Delta t} = \frac{\lambda}{\rho \cdot c_p} \cdot \left(\frac{1}{r} \cdot \frac{T_{i+1}^n - T_{i-1}^n}{2\Delta r} + \frac{T_{i+1}^n - 2T_i^n + T_{i-1}^n}{\Delta r^2}\right) - \frac{\Delta H_R \cdot \dot{M}_{v,CO_2}}{\rho \cdot c_p} \tag{17}$$

The discretized form of the two boundary conditions, Eqs. (12) and (13) are given respectively by Eqs. (18) and (19);

$$-\lambda \cdot \frac{T_s^n - T_{N-1}^n}{2\Delta r} = \left(\sigma \cdot \varepsilon \cdot \left(T_F^4 - T_s^{n\,4}\right) - \alpha_{conv} \cdot \left(T_s^n - T_g\right)\right) \tag{18}$$

$$T_1^n = T_2^n \tag{19}$$

5. Result and Discussion

5.1 Decomposition Behaviour

Figs. 3a and 3c are temperature and conversion profiles recorded experimentally for the decomposition of 32 mm cylindrical samples in steps 1 and 2 respectively at an ambient temperature of 865°C and 990°C. The decomposition of only $MgCO_3$ is possible in step 1 because the ambient CO_2 partial pressure is 1 bar which is above the equilibrium partial pressure of $CaCO_3$ decomposition and less than the partial pressure of CO_2 in the porous layer formed during $MgCO_3$ decomposition. Considering Fig. 3a, an initial rapid rise in core temperature is seen up to 720°C after 10 minutes, here no reaction is taking place as the equilibrium pressure is low and the heat transported to the sample is consumed in raising the sample's internal energy. However, comparing the two curves a conversion of about 20% is observed at 10 minutes, which is because the sample surface reaches the decomposition temperature before the core and some degree of reaction has been reached in this period. The temperature then remains steady at 720°C where a high enough equilibrium pressure is reached so that the heat transferred to the sample is consumed mainly by reaction and thus a rapid degree of conversion. At the end of calcination, core temperature of the sample rises until equilibrium with the ambient is reached. The description given above also applies to the second stage of dolomite decomposition as seen in Fig. 3c. The first and second stages of dolomite decomposition are similar to the decomposition of pure magnesite and calcite when the calcination temperatures are compared which is remarkable considering the presence of the $CaCO_3$ in step 1 and the MgO in step 2. For both steps, when the ambient temperature is increased, decomposition temperature is higher and thus faster decomposition is recorded.

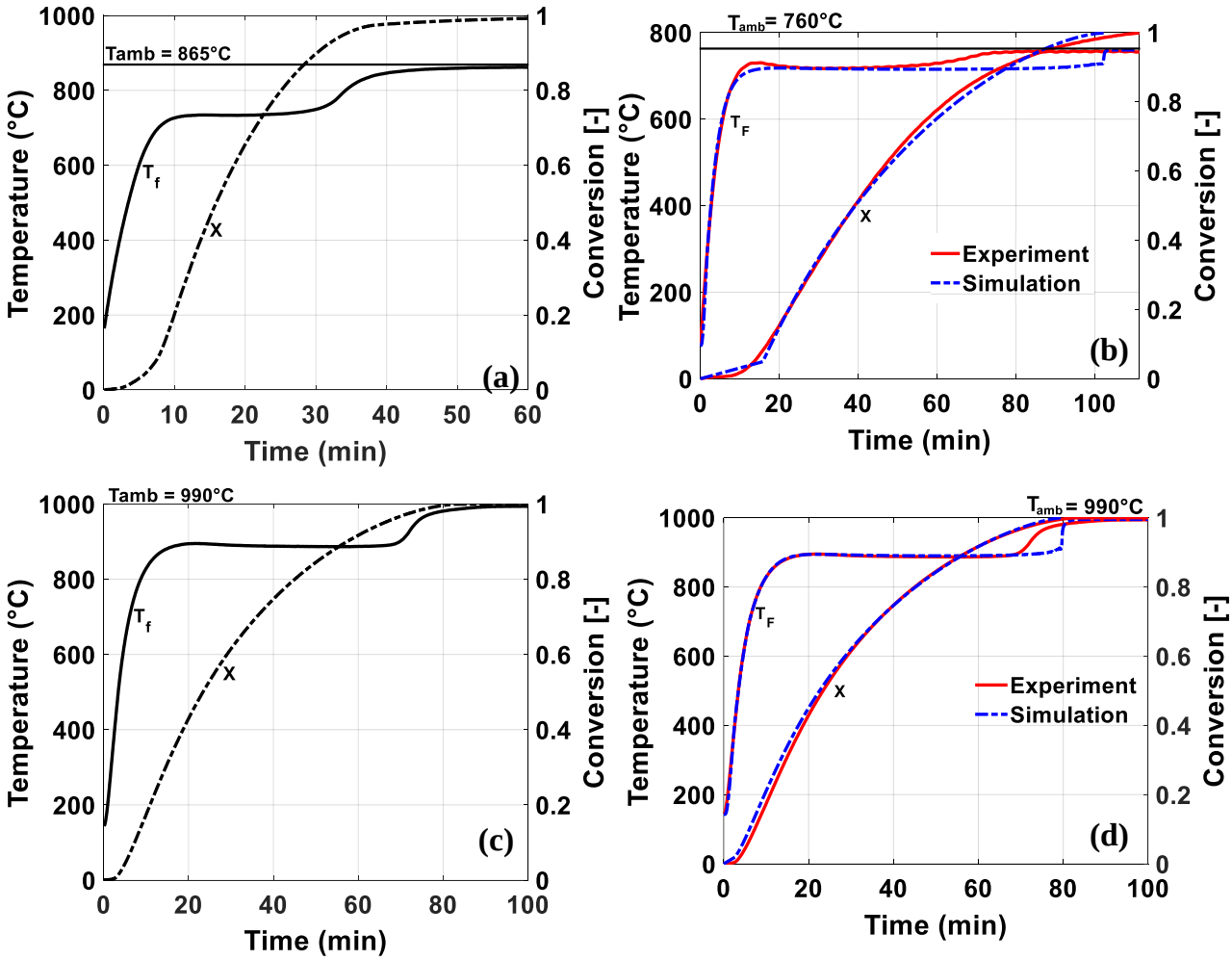

Fig. 3: Core temperature and conversion profile in (a) the first step of 32 mm cylindrical dolomite decomposition at an ambient temperature of 865°C (c) the second step of 32 mm cylindrical half burnt dolomite decomposition at an ambient temperature of 990°C and Comparison between experimentally measured and calculated temperature and conversion profiles for (b) 24 mm cylindrical dolomite sample decomposed at 760°C ambient temperature (d) 32 mm cylindrical half burnt dolomite sample decomposed at 990°C ambient temperature.

5.2 Model Validation with Experiment

The decomposition process was simulated based on the model described in chapter 2 and the predicted temperature and conversion profiles were compared with that experimentally recorded (see Figs. 3b and 3d). The model predicts quite well the decomposition behaviour of the $CaCO_3$ part of dolomite (step 2) as seen by the matching curves in Fig. 3d. For the decomposition of $MgCO_3$ (step 1), even though the predicted initial rapid rise in temperature, decomposition temperature and time of decomposition agree with that experimentally recorded, Fig. 3b show the measured temperature profile begins to rise at 50 minutes after a conversion of 65% has been reached while the predicted profile remains constant. Two reasons, which the model does not accounted for, can be given for the deviation; the presence of reaction zones as well as the assumed reaction layer or the heat transferred to the sample is higher than needed after 65% of the carbonate has been decomposed.

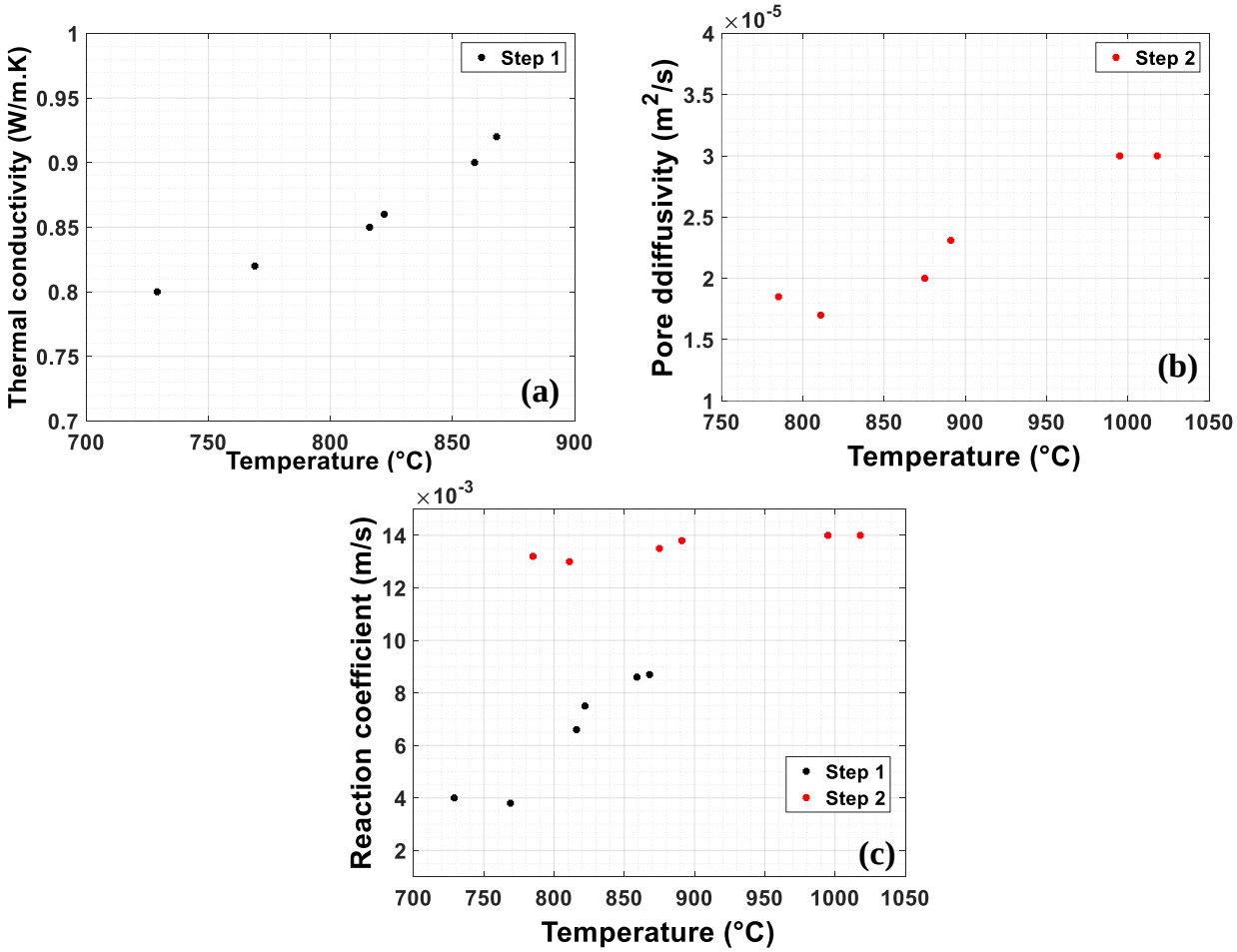

Fig. 4: (a) Temperature dependence of thermal conductivity of $MgO{\cdot}CaCO_3$ (b) Temperature dependence of the pore diffusivity $MgO{\cdot}CaO$ (c) Temperature dependence of reaction coefficient in steps 1 and 2.

5.3 Material values

The values used in the model that give the best match of the predicted and measured profiles were taken as the approximate thermophysical material properties. The estimated values are shown as a function of ambient temperature in Fig. 4. In step 1, when the ambient temperature is increased from 730 to 860°C, the thermal conductivity of porous $MgO{\cdot}CaCO_3$ slightly increases from 0.79 to 0.92 W/m·K (Fig. 4a), while the permeability is estimated to be 1 x 10^{-12} m^2 and the reaction coefficient is in the range of 0.0040 to 0.0085 m/s (Fig. 4c). In step 2, for ambient temperatures between 790 and 1020°C, the thermal conductivity of porous $MgO{\cdot}CaO$ is estimated to be 0.8 W/m.K, the pore diffusion coefficient is almost doubled from 1.7 x 10^{-5} to 3.0 x 10^{-5} m^2/s (Fig. 4b) and the reaction rate coefficient displayed no significant temperature dependence with values between 0.013 and 0.014 m/s (Fig. 4c). The reported values are comparable to those reported for the decomposition of pure $CaCO_3$ [14] in step 2 and pure magnesite in step 1 [15].

6. Conclusion

Dolomite samples of size 24 and 32 mm in cylindrical form were decomposed in two stages and the recorded behaviour is seen to be identical to those of pure $MgCO_3$ and $CaCO_3$. Thermophysical properties of $MgO{\cdot}CaCO_3$ and $MgO{\cdot}CaO$ were evaluated by numerically solving the heat and mass balance equations describing the decomposition process. The results show that permeability of porous $MgO{\cdot}CaCO_3$ is independent of

temperature, while the thermal conductivity and reaction coefficient only slightly depend on temperature. The thermal conductivity of MgO·CaO does not change with temperature and the pore diffusion coefficient and reaction rate coefficient show no significant temperature dependence.

References

[1] J. M. Valverde, A. Perejon, S. Medina, and L. A. Perez-Maqueda, ‘‘Thermal decomposition of dolomite under CO_2: insights from TGA and in situ XRD analysis,’’ *Phys. Chem. Chem. Phys.*, vol. 17, no. 44, pp. 30162–30176, 2015.

[2] P. G. Caceres and E. K. Attiogbe, ‘‘Thermal decomposition of dolomite and the extraction of its constituents,’’ *Minerals Engineering*, vol. 10, no. 10, pp. 1165–1176, 1997.

[3] F. D. M. Daud, K. Vignesh, S. Sreekantan, and A. R. Mohamed, ‘‘Improved CO_2 adsorption capacity and cyclic stability of CaO sorbents incorporated with MgO,’’ *New J. Chem.*, vol. 40, no. 1, pp. 231–237, 2016.

[4] K. O. Albrecht, K. S. Wagenbach, J. A. Satrio, B. H. Shanks, and T. D. Wheelock, ‘‘Development of a CaO-Based CO_2 Sorbent with Improved Cyclic Stability,’’ *Ind. Eng. Chem. Res.*, vol. 47, no. 20, pp. 7841–7848, 2008.

[5] S. Senthoorselvan, S. Gleis, S. Hartmut, P. Yrjas, and M. Hupa, ‘‘Cyclic carbonation calcination studies of limestone and dolomite for CO_2 separation from combustion flue gases,’’ *Journal of Engineering for Gas Turbines and Power*, vol. 131, 2009.

[6] H. Galai, M. Pijolat, K. Nahdi, and M. Trabelsiayadi, ‘‘Mechanism of growth of MgO and CaCO3 during a dolomite partial decomposition,’’ *Solid State Ionics*, vol. 178, no. 15–18, pp. 1039–1047, 2007.

[7] M. Olszak-Humienik and M. Jablonski, ‘‘Thermal behavior of natural dolomite,’’ *J Therm Anal Calorim*, vol. 119, no. 3, pp. 2239–2248, 2015.

[8] S. Gunasekaran and G. Anbalagan, ‘‘Thermal decomposition of natural dolomite,’’ Bull. Mater. Sci., vol. 30, no. 4, pp. 339-344, 2007.

[9] H. Kainer, ‘‘Kopplung von Wärme- und Stoffaustausch mit chemischer Kinetik bei der Zersetzung von natürlichen Karbonaten - Teil II,’’ Ph.D. dissertation, Fakultät für Bergbau, Hüttenwessen, und Maschinenwesen, TU Clausthal, 1982.

[10] R. M. McIntosh, J. H. Sharp, and F. W. Wilburn, ‘‘The thermal decomposition of dolomite,’’ *Thermochimica Acta*, vol. 165, no. 2, pp. 281–296, 1990.

[11] D. T. Beruto, R. Vecchiattini, and M. Giordani, ‘‘Solid products and rate-limiting step in the thermal half decomposition of natural dolomite in a CO2 (g) atmosphere,’’ *Thermochimica Acta*, vol. 405, no. 2, pp. 183–194, 2003.

[12] A. B. Fuertes, G. Marban and F. Rubiera, ‘‘Kinetics of thermal decomposition of limestone particles in a fluidized bed reactor,’’ Trans. IChemE, vol 71, part A, pp. 421–428, 1993.

[13] P. C. G. Sandaka, ‘‘Calcination behavior of lumpy limestones from different origins,’’ Ph.D. dissertation, Fakultät für Verfahrens- und Systemtechnik, Otto-von-Guericke-Universität, Magdeburg, 2015.

[14] H. Kainer, E. Specht, R. Jeschar, ‘‘*Die Poreendiffusions-,Reaktions- und Wärmelritkoeffizienten verschidener Kalksteine und ihr Einfluß auf die Zersetzungszeit*,’’ Zement-Kalk-Gips, vol. 5, pp. 259-268, 1986.

[15] H. Kainer, E. Specht, R. Jeschar, ‘‘*Die Poreendiffusions-,Reaktions- und Wärmelritkoeffizienten verschidener Magnesite und ihr Einfluß auf die Zersetzungszeit*,’’ Radex-Rundschau, vol. 4, pp. 248-268, 1986.